Supplementary Figure 1 (A-G)

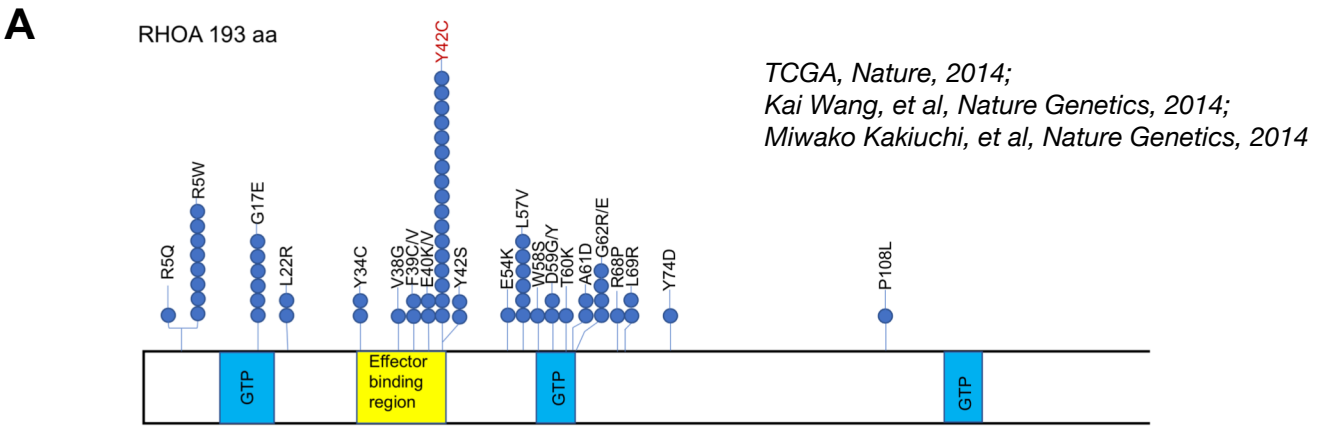

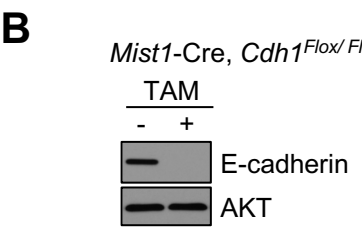

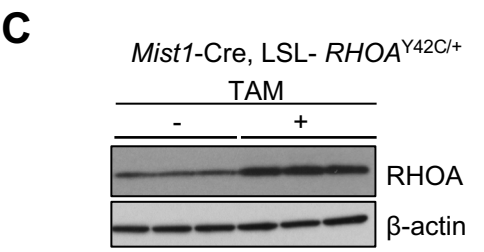

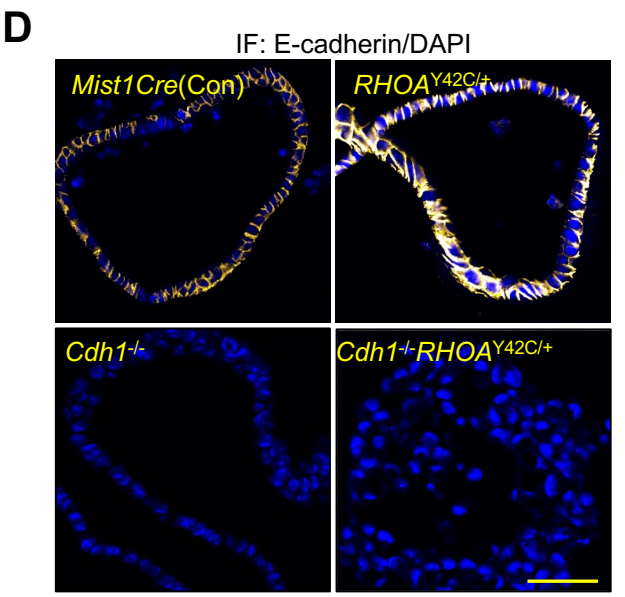

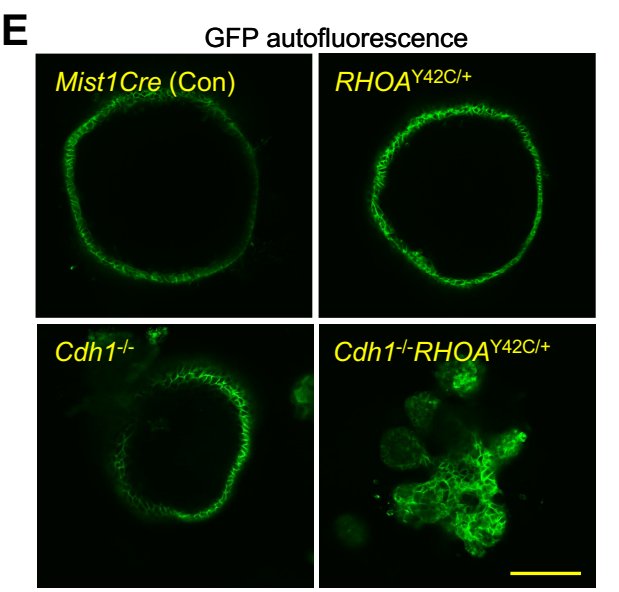

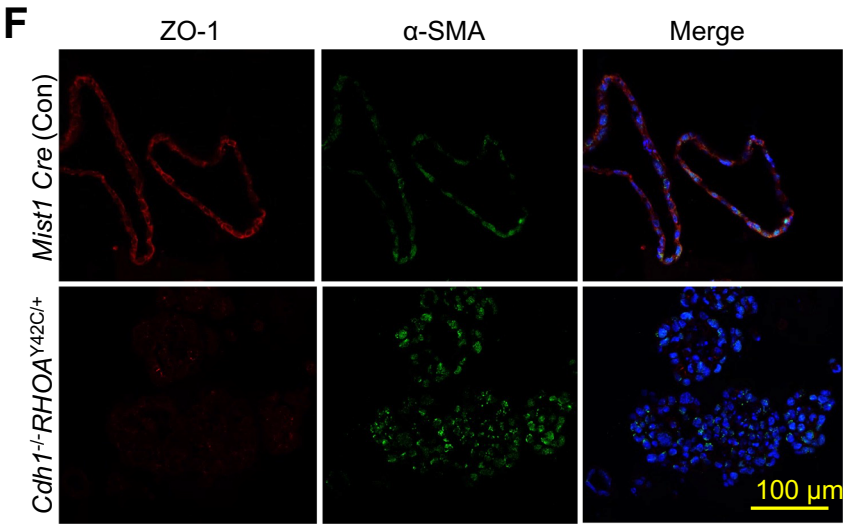

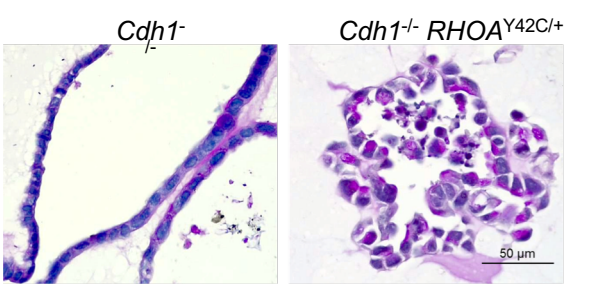

Supplementary Figure 1 (H-K)

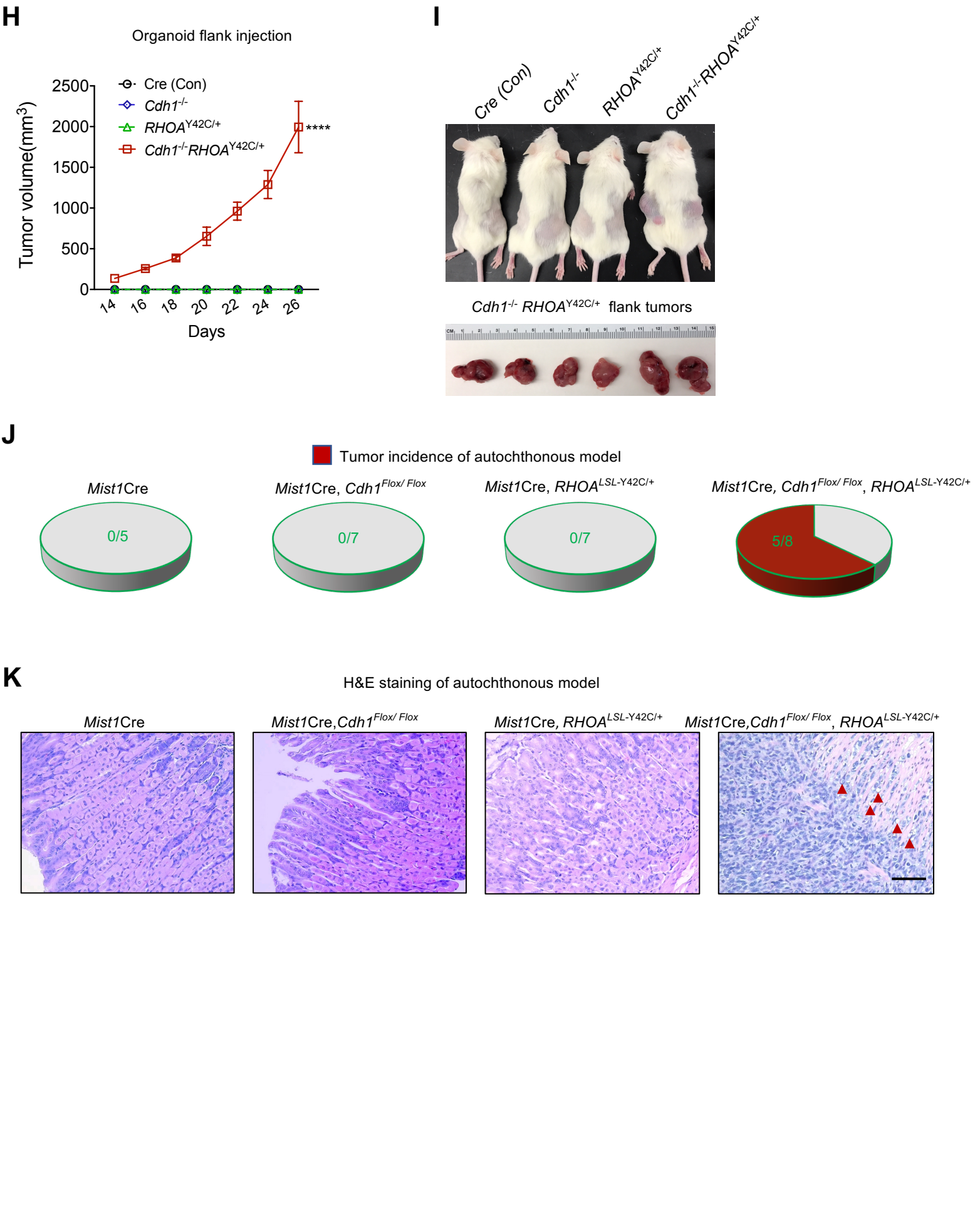

Supplementary Figure 1. Model the pathogenesis of diffuse gastric cancer

A, Spectrum of RHOA mutations in gastric cancers, compiled from TCGA and two contemporaneous reports identifying these alterations. Immunoblots of E-cadherin (**B**) and RHOA (**C**) in organoids treated with or without tamoxifen (2 μM) for 96 h (n = 3 independent experiments). **D,** Representative confocal immunofluorescence images of E-cadherin in the annotated organoids. Scale bar = 50 μm. **E,** Representative confocal images of GFP autofluorescence in the annotated organoids. Scale bar = 100 μm. **F,** Confocal immunofluorescence images of ZO-1 and α-SMA in the indicated organoids. Scale bar = 100 μm. **G,** Periodic acid-Schiff (PAS) staining of paraffin sections of the indicated organoids. Scale bar = 50 μm. **H,** Tumor volumes following NSG flank implantation of organoids with annotated genotypes, showing tumor formation only by *Cdh1*$^{-/-}$*RHOA*$^{Y42C/+}$ organoids. Data are mean ± S.E.M., ****P<0.0001, two-way ANOVA (*Cdh1*$^{-/-}$*RHOA*$^{Y42C/+}$ versus other genotypes). **I,** Representative images of NSG flank tumors in panel (**H**).

J, Autochthonous tumor incidence in mice with annotated genotypes following 3 rounds of tamoxifen induction starting at 6-8 weeks of age. **K,** Representative H&E images of gastric tissue with autochthonous induction of distinct alleles. Samples obtained 14 months following tamoxifen induction. Red arrows: cells resembling signet-ring cells. Scale bar = 100 μm.

Supplementary Figure 2

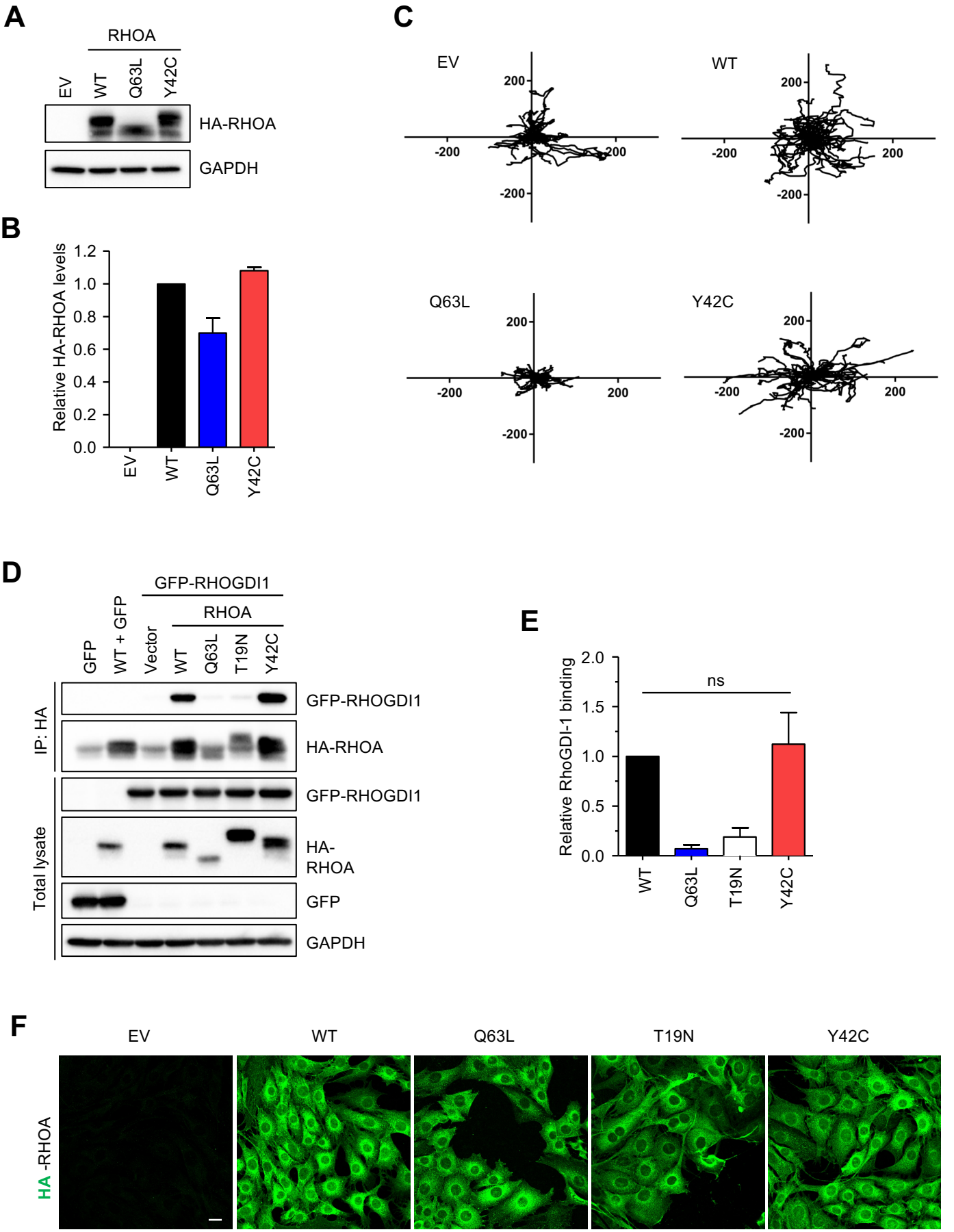

Supplementary Figure 2. Cellular and biochemical properties of RHOA^{Y42C}

Immunoblot analyses of NIH/3T3 fibroblasts stably expressing exogenous HA epitope-tagged RHOA proteins, using anti-HA to detect HA-RHOA proteins and anti-GAPDH to monitor for equivalent loading of total cellular protein. Blot (**A**) is representative of n = 3. Quantitation (**B**) shows mean data ± S.E.M. **C,** Plots showing the random migration tracks of HA-RHOA-expressing NIH/3T3 cells from Fig. 2G were captured by time lapse microscopy. Data are representative of n = 4 (25 cells per experiment). COS-7 cells transiently co-expressing HA-RHOA and/or EGFP-RHOGDI1 were used for immunoprecipitation analyses with anti-HA epitope-conjugated agarose beads to monitor the amount of co-precipitating GFP-RHOGDI using a GFP antibody. Blot (**D**) is representative of n = 3. Quantitation (**E**) shows mean data ± S.E.M. ns, not significant; unpaired two-tailed *t*-test**. F,** Immunofluorescence images of NIH/3T3 cells stably expressing HA-RHOA proteins. Images are representative of two independent experiments. Scale bar = 20 µm.

Supplementary Figure 3

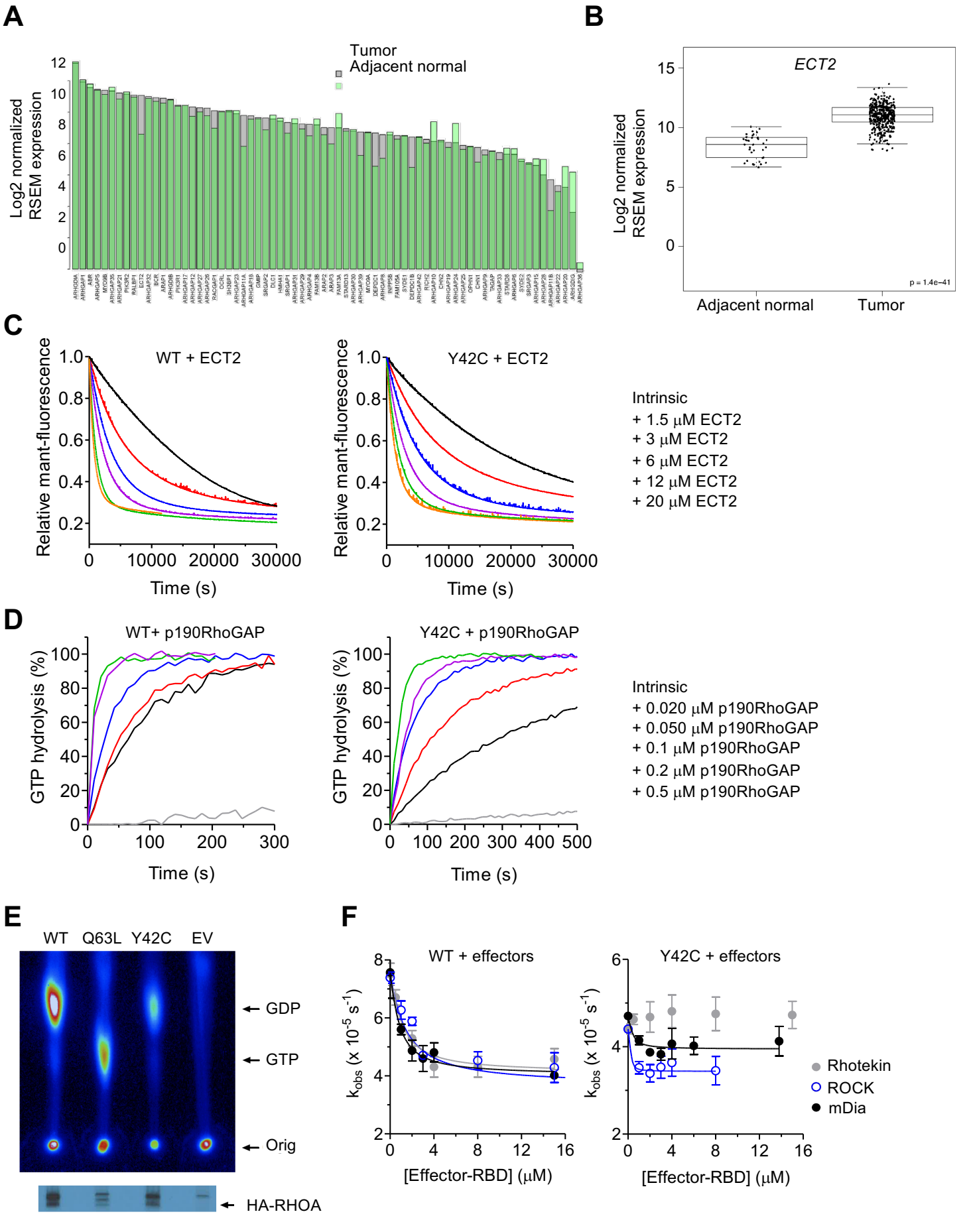

Supplementary Figure 3. Expression analysis of RHOA and its regulators, and the mechanistic basis of RHOA^{Y42C}

(**A**) RhoGEF and RhoGAP expression data from TCGA. Median expression values for genes were plotted for tumors (n=415) and cancer adjacent normals (n=35) and ordered by median expression level in tumors. (**B**) Box plot of gene expression values for *ECT2* in TCGA tumors and cancer-adjacent normal. (**C**) Kinetics of intrinsic and RhoGEF ECT2-catalyzed RHOA nucleotide exchange on RHOA WT (left) and RHOA^{Y42C} (right). Data shown are representative of three independent experiments. Observed rates k_{obs} to determine kcat are in Fig. 3B. (**D**) Kinetics of the intrinsic and p190RhoGAP-stimulated GTP hydrolysis activities of RHOA WT (left panel) and RHOA^{Y42C} (right panel) of a representative GAP assay, using indicated GAP concentrations and the phosphate binding protein sensor. Observed rates k_{obs} to determine kcat are in Fig. 3G. (**E**) NIH/3T3 cells stably expressing HA-RHOA were used for metabolic ^{32}P labeling. HA-RHOA proteins were isolated by immunoprecipitation with anti-HA epitope-conjugated agarose beads. Incorporated ^{32}P signal of HA-RHOA bound GDP and GTP was detected by thin-layer chromatography and phosphor imaging (top). To monitor for equal HA-RHOA expression, cells were in parallel labeled with ^{35}S methionine, followed by immunoprecipitation of HA-RHOA and immunoblot analyses with anti-HA (bottom). Blots are representative of two independent experiments. (**F**) RHOA binding affinities to the RBDs of Rhotekin, ROCK and mDia (concentrations as indicated) were measured based on the observed rate k_{obs} of the inhibition of the mantGppNHp nucleotide dissociation (GDI effect, n = 3). Data are mean ± S.E.M**.**

Supplementary Figure 4 (A-F)

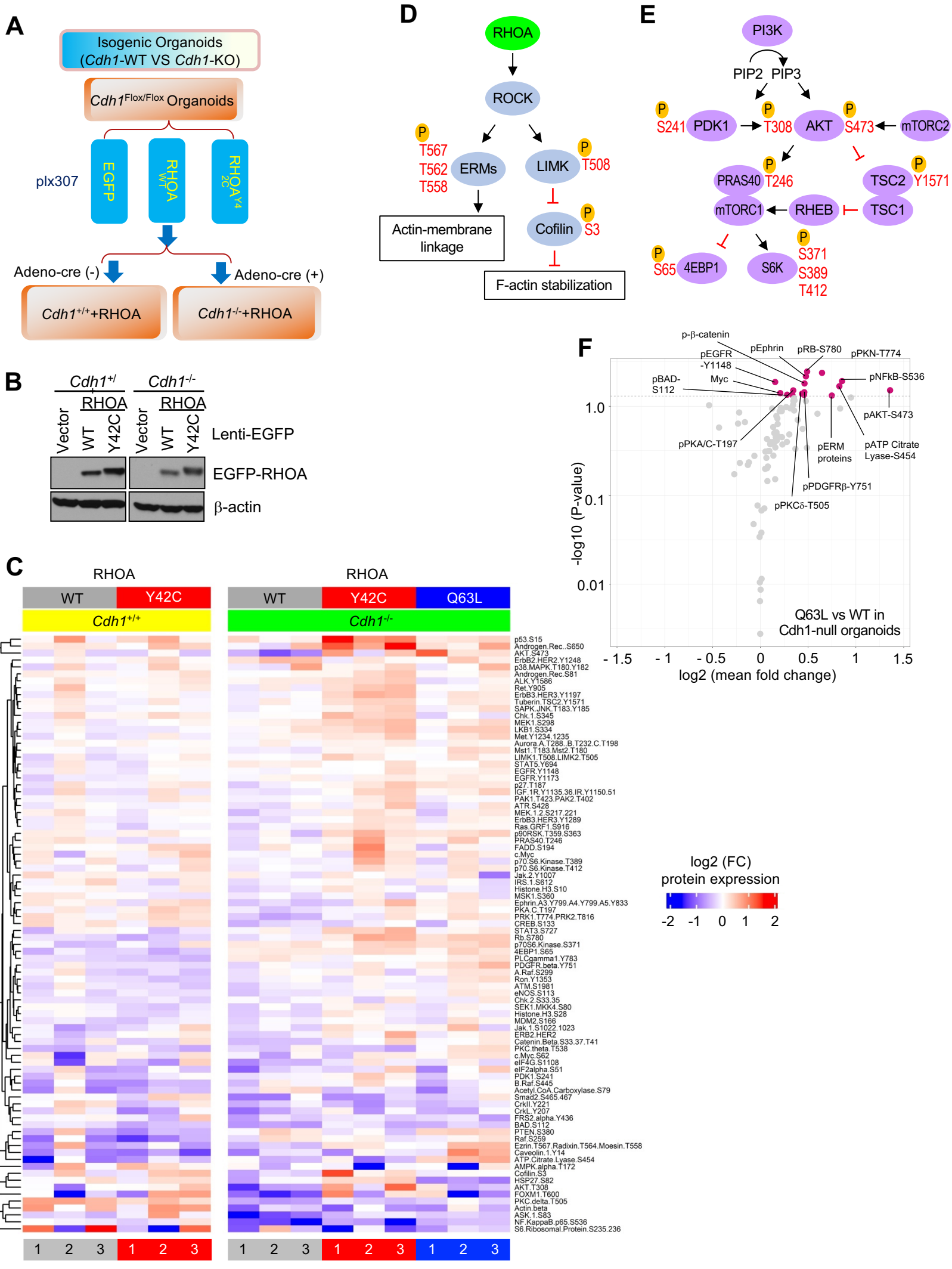

Supplementary Figure 4 (G-P)

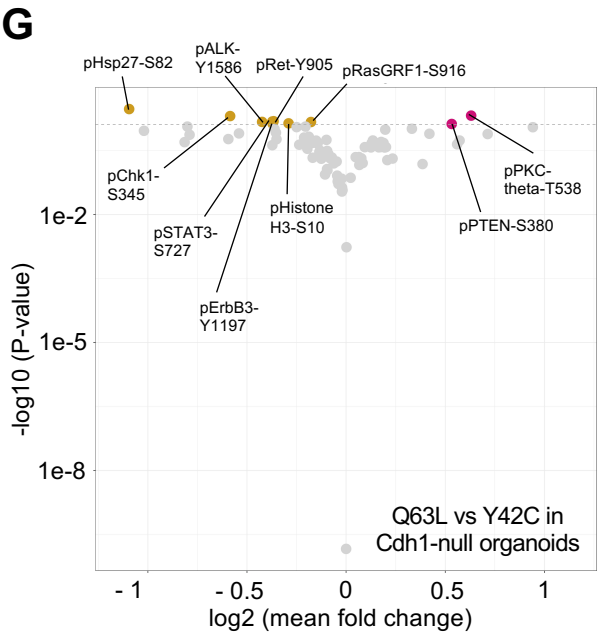

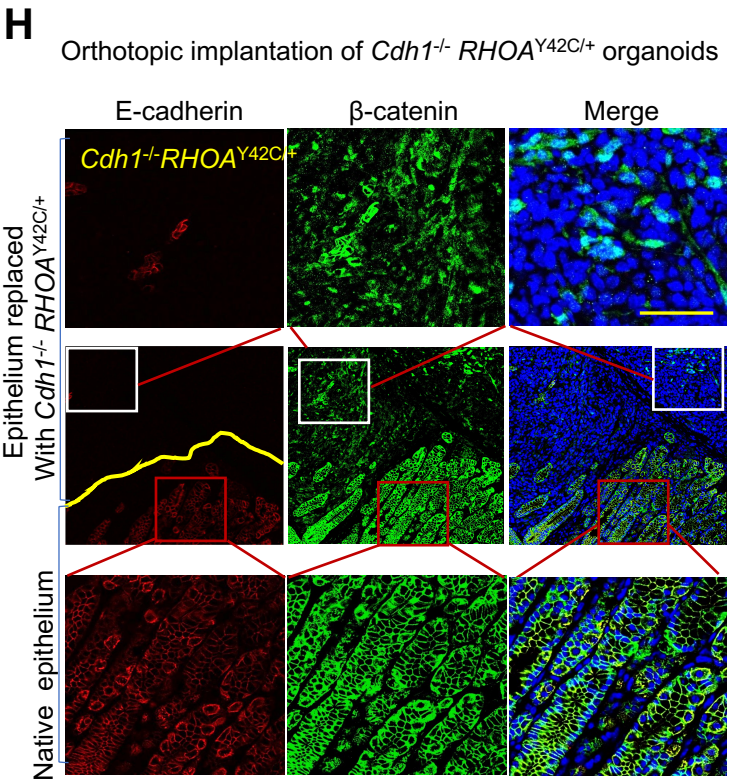

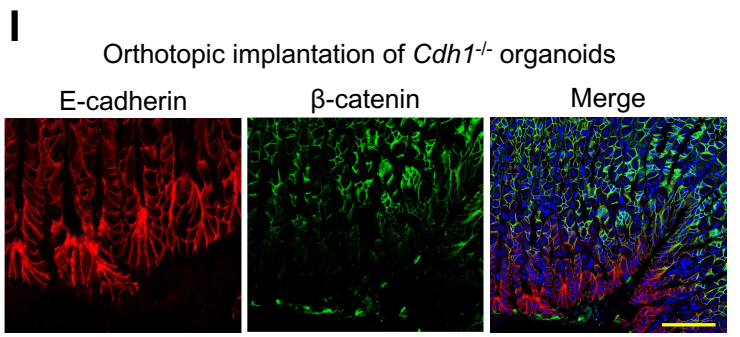

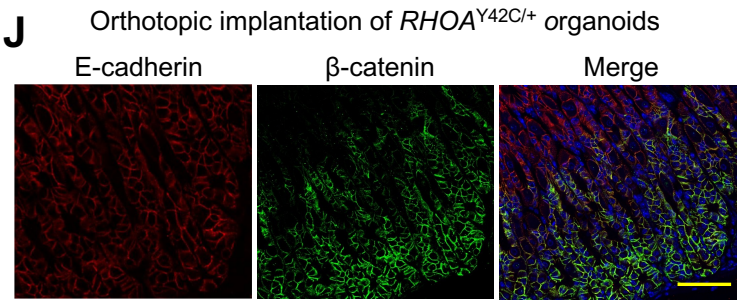

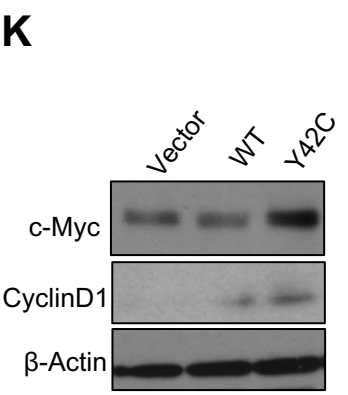

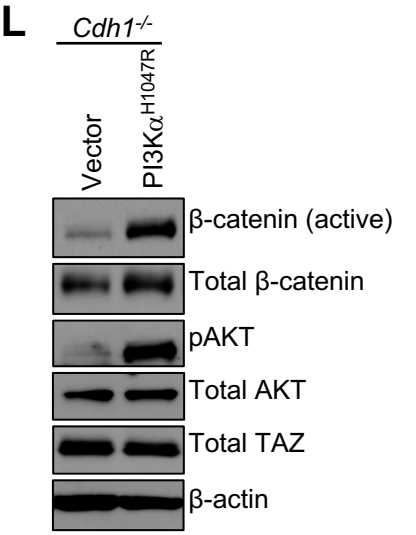

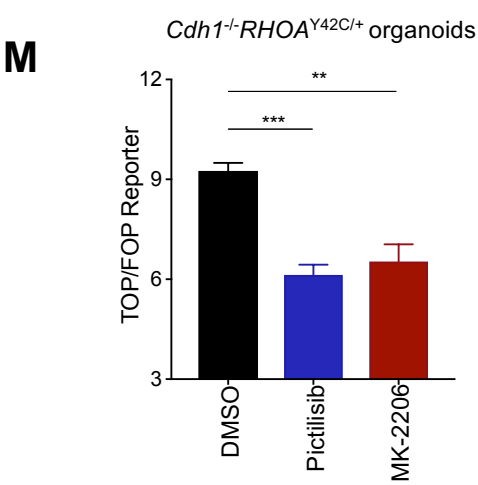

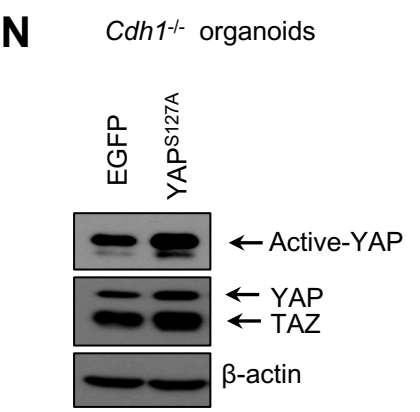

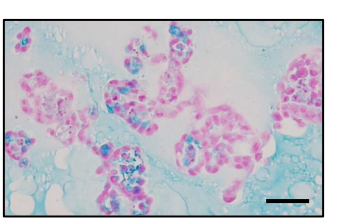

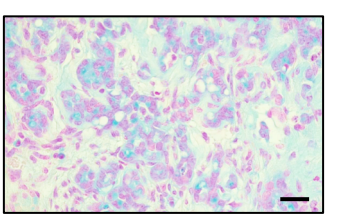

Supplementary Figure 4. *Cdh1* loss and RHOA-Y42C induces AKT and β-catenin activation

(**A**) Schematic for the generation of isogenic organoids with or without *Cdh1* loss and engineered with lenti-EGFP-RHOA^{-Y42C} or controls. (**B**) Representative immunoblotting for ectopic lenti-RHOA expression in isogenic organoids from panel (**A**) (n = 3 independent experiments). (**C**) All antibodies from RPPA analysis of isogenic gastric organoids with annotated genotypes. *Cdh1*$^{+/+}$ and *Cdh1*$^{-/-}$ fold change values were calculated with respect to matched RHOA-EV controls per antibody. Resulting values were log2 changed and clustered using k-means clustering for antibodies. Confocal immunofluorescence images for E-cadherin and β-catenin in NSG stomach epithelium injected with *Cdh1*$^{-/-}$*RHOA*$^{Y42C/+}$ organoids (**D-E**) Models depicting proteins in RPPA antibody panel involved in (**D**) ROCK effector signaling and in (**E**) PI3K-AKT-mTORC1 signaling (see Fig. 4A). (**F, G**) Volcano plot representing RPPA results (**F**) comparing RHOA^{Q63L} versus RHOA^{WT} in Cdh1-null organoids or (**G**) comparing RHOA^{Q63L} versus RHOA^{Y42C} in Cdh1-null organoids. Significantly upregulated and downregulated proteins and phosphorylation sites are represented by pink and gold dots, respectively. Horizontal dotted line represents p-value threshold of 0.05. List of top hits is shown in Supplementary Table S1. (**H**) Bottom: native epithelium with normal E-cadherin and β-catenin in the cytoplasm. Top: epithelium replaced by *Cdh1*$^{-/-}$*RHOA*$^{Y42C/+}$ organoids, with E-cadherin loss and β-catenin translocated into nucleus, scale bar= 50 μm, or injected by *Cdh1*$^{-/-}$ organoids (**I**) or by *RHOA*$^{Y42C/+}$ organoids (**J**). Scale bar = 100 μm. (**K**) Immunoblotting for c-Myc and CyclinD1 in *Cdh1*-null organoids with lentiviral EGFP-RHOA^{Y42C} or controls (representative image from 3 independent experiments). (**L**) Immunoblots of *Cdh1*$^{-/-}$ organoids with ectopic expression of lenti-EGFP or lenti-PIK3CA (H1047R) (n = 3 independent experiments). (**M**) TOP/FOP Wnt/β-catenin reporter assay in *Cdh1*$^{-/-}$*RHOA*$^{Y42C/+}$ cells treated with DMSO, PI3K inhibitor pictilisib (2 μM) or AKT inhibitor MK-2206 (2 μM) for 24 h. Data are mean ± S.E.M. ***P*<0.01, ****P*<0.001, unpaired two-tailed Student's *t*-test. (**N**) Immunoblots of *Cdh1*$^{-/-}$ organoids infected with lenti-EGFP or active YAP (S127A). Image is representative of n = 3 independent experiments. (**O**) Representative image of Alcian blue staining of the *Cdh1*-null organoids with ectopic expression of YAP(S127A) and β-catenin(S33Y), Scale bar = 100 μm. (**P**) Representative image of Alcian blue staining for the tumor from Fig. 4H. Scale bar = 100 μm.

Supplementary Figure 5

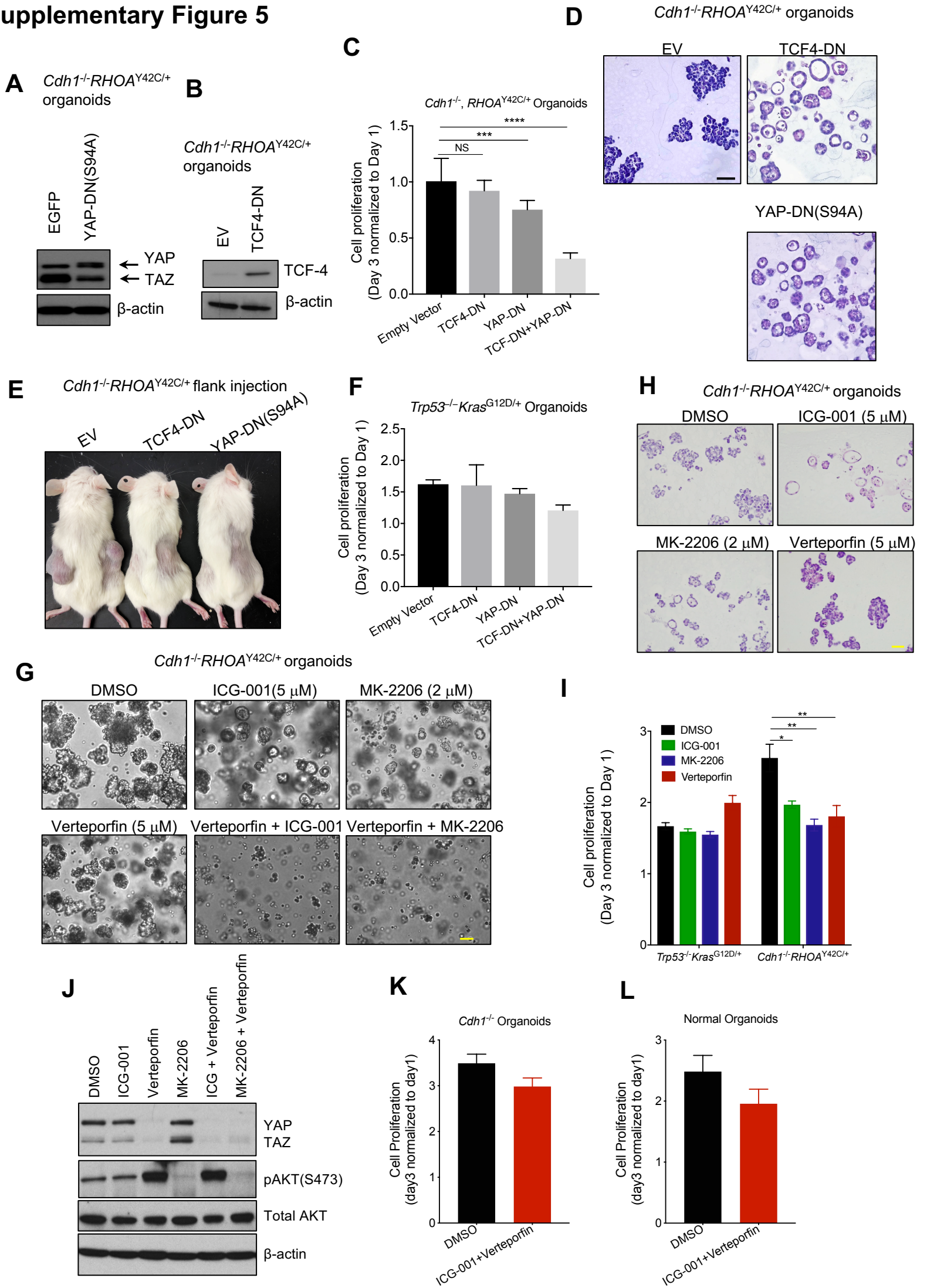

Supplementary Figure 5. Wnt and YAP pathways are both required for the transformation of *Cdh1*$^{-/-}$*RHOA*$^{Y42C/+}$ organoids

(**A**) Immunoblots of *Cdh1*$^{-/-}$*RHOA*$^{Y42C/+}$ organoids infected with lenti-EGFP or dominant negative YAP (S94A). Image is representative of n = 3 independent experiments. (**B**) Immunoblots of *Cdh1*$^{-/-}$ *RHOA*$^{Y42C/+}$ organoids infected with EV or dominant negative β-catenin cofactor TCF4 [TCF-DN (aa 1-31 del)]. (**C**) *In vitro* proliferation (CellTiter-Glo) of *Cdh1*$^{-/-}$*RHOA*$^{Y42C/+}$ organoids with ectopic expression of TCF4-DN (aa 1-31 del), YAP-DN (S94A) or combination. Data are mean ± S.E.M., ***P<0.001, ****P<0.001, NS: not significant, unpaired two-tailed Student's t-test. (**D**) Representative H&E images of *Cdh1*$^{-/-}$*RHOA*$^{Y42C/+}$ organoids infected with EV, TCF-DN or YAP-DN . Scale bar = 100 μm. (**E**) Representative images of NSG flank tumors generated from *Cdh1*$^{-/-}$*RHOA*$^{Y42C/+}$ organoids with EV, TCF4-DN or YAP-DN. (**F**) *In vitro* proliferation (CellTiter-Glo) of *Trp53*$^{-/-}$*Kras*$^{G12D/+}$ organoids with ectopic expression of TCF4-DN, YAP-DN or combination. Data are mean ± S.E.M. Comparisons (no significance) were made between EV and genetic perturbation groups using unpaired two-tailed Student's t-test. Representative images of phase contrast (**G**) and H&E staining (**H**) of *Cdh1*$^{-/-}$*RHOA*$^{Y42C/+}$ organoids treated for 48 h with DMSO, ICG-001 (antagonist of β-catenin/TCF4 binding, 5 μM), MK-2206 (AKT inhibitor, 2 μM), verteporfin (YAP inhibitor, 5 μM) or the indicated combinations. Scale bar = 100 μm. (**I**) *In vitro* proliferation (CellTiter-Glo) of *Cdh1*$^{-/-}$*RHOA*$^{Y42C/+}$ or *Trp53*$^{-/-}$*Kras*$^{G12D/+}$ organoids treated for 48 h with DMSO or ICG-001 (5 μM), MK-2206 (2 μM) or verteporfin (5 μM). Data are mean ± S.E.M. *P<0.05, **P<0.01, unpaired two-tailed Student's *t*-test. (**J**) Representative immunoblots of *Cdh1*$^{-/-}$*RHOA*$^{Y42C/+}$ organoids treated for 24 h with DMSO or ICG-001 (5 μM), MK-2206 (2 μM) or verteporfin (5 μM), or the indicated combinations (n = 3 independent experiments). (**K-L**) *In vitro* proliferation (CellTiter-Glo) of *Cdh1*$^{-/-}$ (**K**) or normal (**L**) organoids treated for 48 h with DMSO or ICG-001 (5 μM) combined with verteporfin (5 μM). Data are mean ± S.E.M. No significance, unpaired two-tailed Student's *t*-test.

Supplementary Figure 6

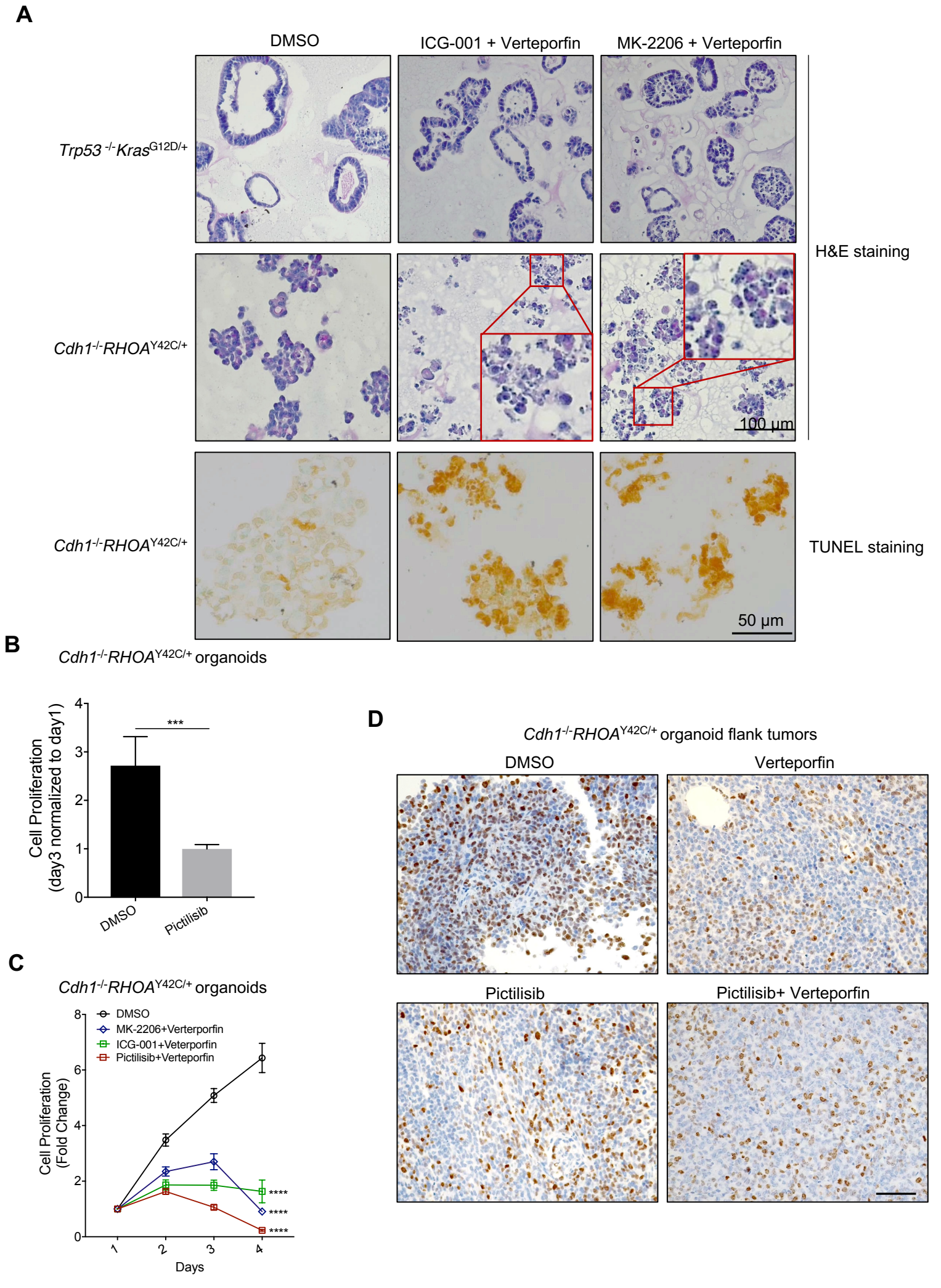

Supplementary Figure 6. PI3K-AKT inhibition and YAP inhibition specifically induces apoptosis of *Cdh1*$^{-/-}$*RHOA*$^{Y42C/+}$ organoids and inhibits cell proliferation

(**A**) Representative images of H&E staining of *Trp53*$^{-/-}$*Kras*$^{G12D/+}$ organoids (top) or *Cdh1*$^{-/-}$*RHOA*$^{Y42C/+}$ organoids (middle) and TUNEL staining (bottom) of *Cdh1*$^{-/-}$*RHOA*$^{Y42C/+}$ organoids treated for 48 h with verteporfin (5 μM) combined with ICG-001 (5 μM) or MK-2206 (2 μM). For TUNEL staining, green: negative for apoptosis; brown: positive for apoptosis. (**B**) *In vitro* proliferation (CellTiter-Glo) of *Cdh1*$^{-/-}$*RHOA*$^{Y42C/+}$ organoids treated with DMSO or PI3K inhibitor pictilisib (2 μM) for 48 h. Data are mean ± S.D. ***P<0.001, unpaired two-tailed Student's t-test. (**C**) *In vitro* proliferation of *Cdh1*$^{-/-}$*RHOA*$^{Y42C/+}$ organoids treated with DMSO or indicated combination (pictilisib, 2 μM; verteporfin, 5 μM; ICG-001, 5 μM; MK-2206, 2 μM). ****P<0.0001, two-way ANOVA (treatment groups versus DMSO). (**D**) Representative images of Ki67 staining of *Cdh1*$^{-/-}$*RHOA*$^{Y42C/+}$ organoid flank tumors treated with DMSO or pictilisib (75 mg/kg), verteporfin (100 mg/kg), or the combination. Scale bar = 100 μm.

Supplementary Figure 7 (A-H)

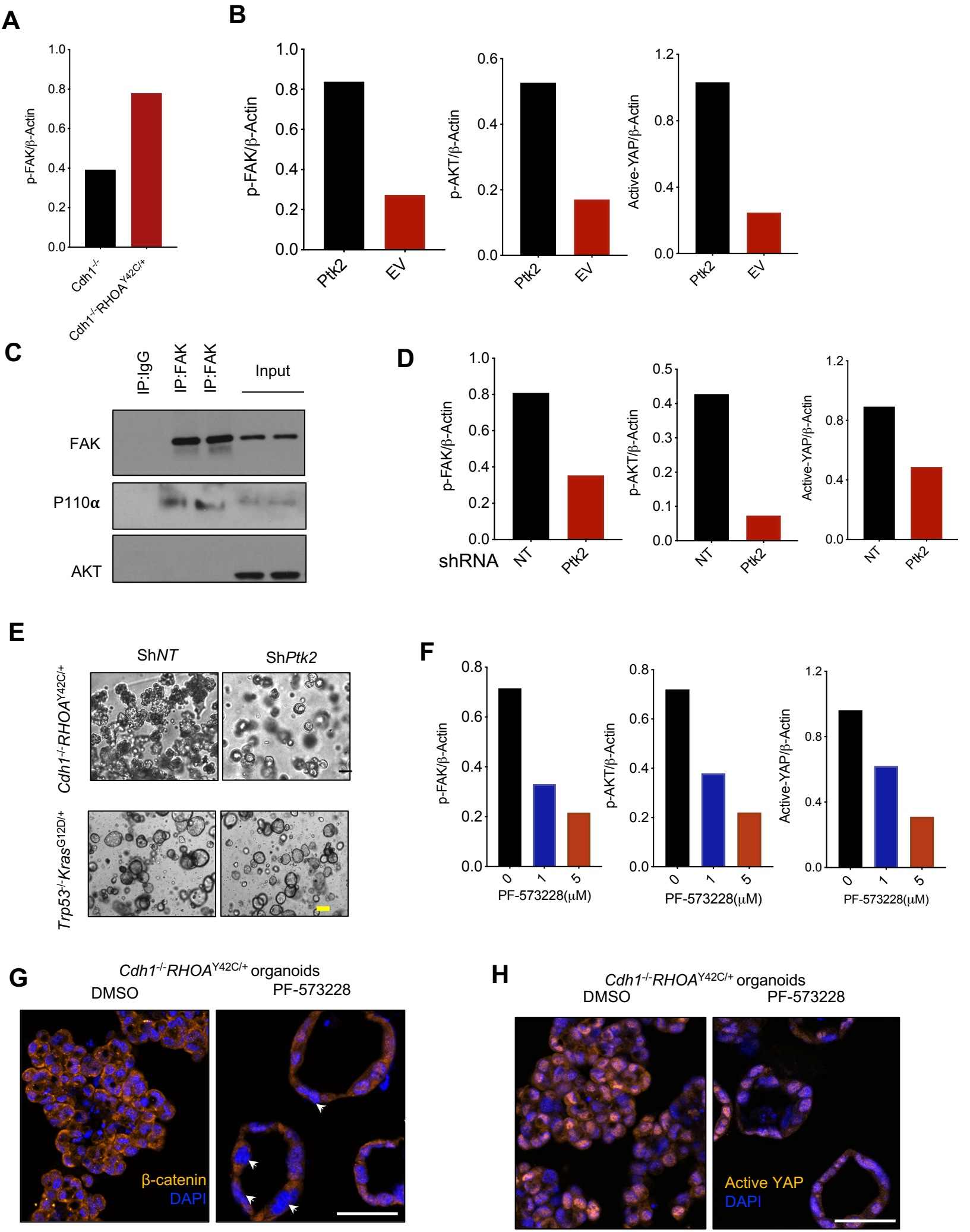

Supplementary Figure 7 (I-R)

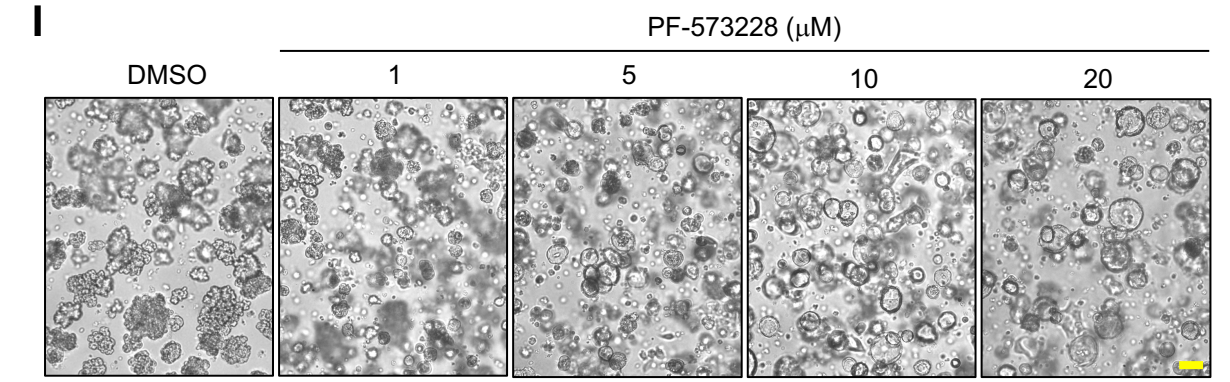

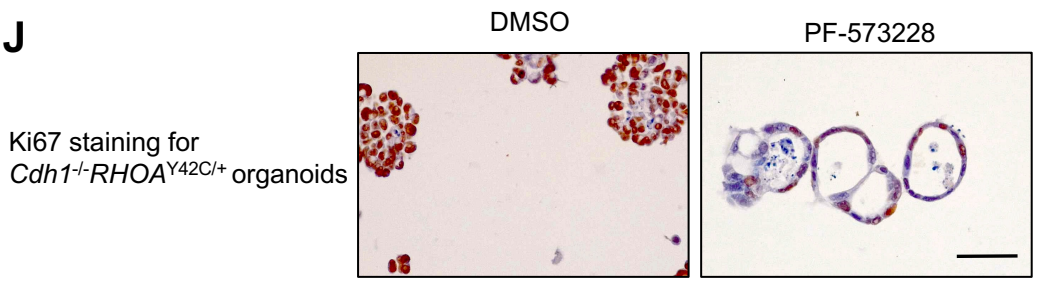

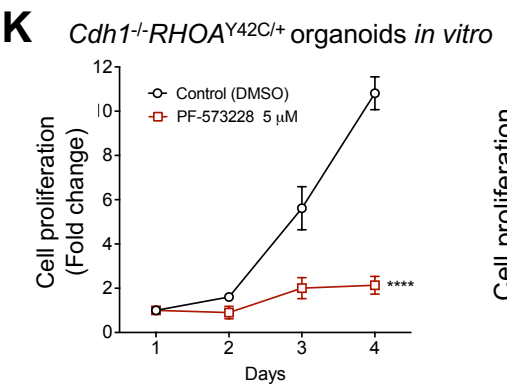

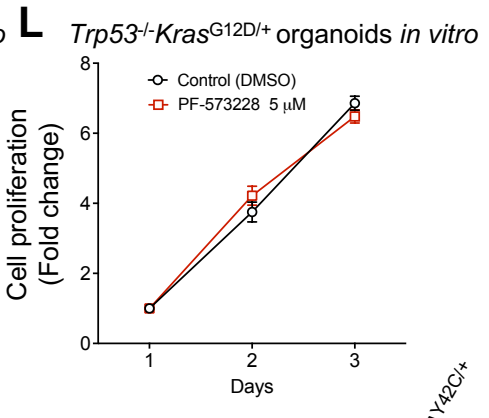

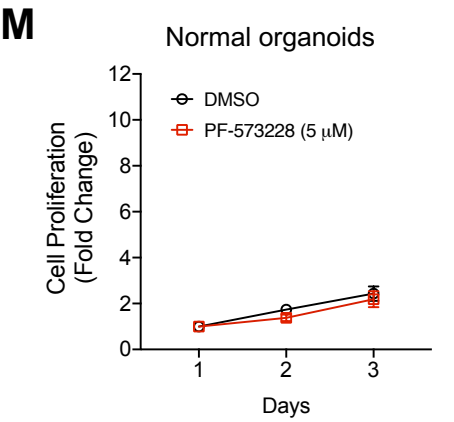

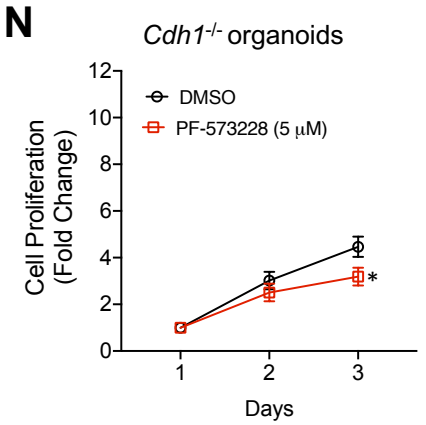

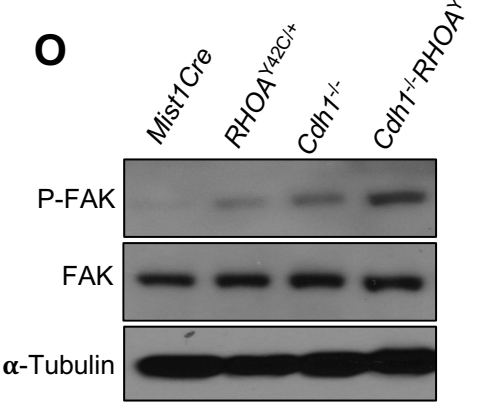

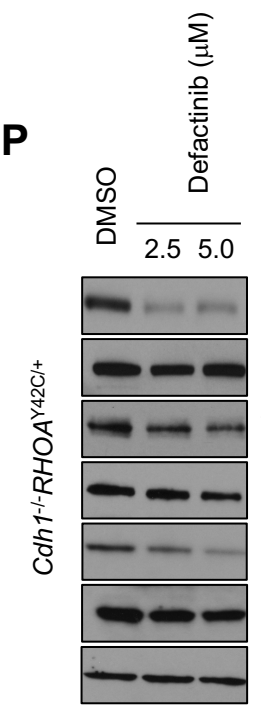

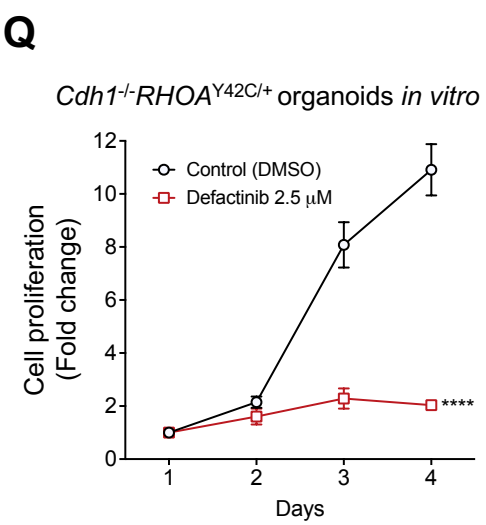

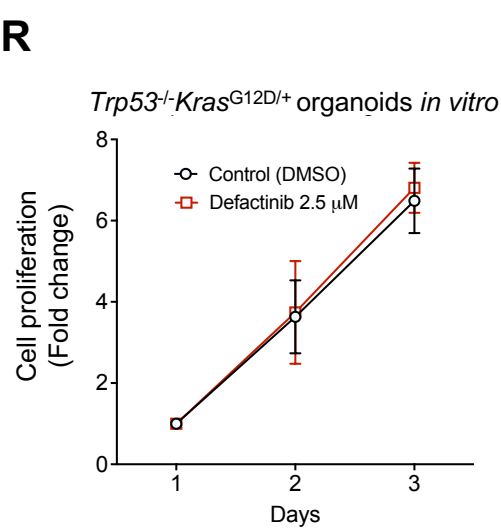

Supplementary Figure 7. FAK is required for *Cdh1*$^{-/-}$*RHOA*$^{Y42C/+}$-induced transformation and for β-catenin and YAP activation.

(**A-B**) Quantitation of Fig.6B and Fig.6C, respectively. (**C**) Immunoblots for P110**α** and AKT of *Cdh1*$^{-/-}$*RHOA*$^{Y42C/+}$ organoids immunoprecipitated with anti-FAK antibody (n = 3 independent experiments). (**D**) Quantitation of Fig.6F.

(**E**) Representative phase contrast images of *Cdh1*$^{-/-}$ *RHOA*$^{Y42C/+}$ organoids or *Trp53*$^{-/-}$ *Kras*$^{G12D/+}$ organoids following *sh*RNA-mediated *Ptk2* (FAK) knockdown or non-targeting control. Scale bar = 100 μm. **(F)**) Quantitation of Fig.6G. (G-H) Confocal immunofluorescence images of (**G**) β-catenin and (**H**) active (non-phosphorylated) YAP in *Cdh1*$^{-/-}$*RHOA*$^{Y42C/+}$ organoids treated as in panel (**C**). Scale bar = 50 μm.

(**I**) Phase contrast images of *Cdh1*$^{-/-}$ *RHOA*$^{Y42C/+}$ organoids treated with DMSO or FAK inhibitor PF-573228 at the indicated doses. Scale bar = 100 μm. (**J**) Representative images of Ki67 staining of *Cdh1*$^{-/-}$*RHOA*$^{Y42C/+}$ organoids treated for 48 h with DMSO or PF-573228 (5 μM). Scale bar = 50 μm. **(K)** *In vitro* proliferation (CellTiter-Glo) of *Cdh1*$^{-/-}$*RHOA*$^{Y42C/+}$ organoids treated for the indicated days with DMSO or PF573228 (5 μM). Data are mean ± S.D. ****P<0.0001, two-way ANOVA. **(L-M)** *In vitro* proliferation of **(L)** *Trp53*$^{-/-}$*Kras*$^{G12D/+}$ or **(M)** normal organoids treated as in panel (**K**). No significance, two-way ANOVA (PF-573228 versus DMSO). Data are mean ± S.D. **(N)** *In vitro* proliferation (CellTiter-Glo) of *Cdh1*$^{-/-}$ organoids treated for the indicated days with DMSO or PF573228 (5 μM). Data are mean ± S.D. *P<0.05, two-way ANOVA. (**O**) Representative immunoblotting of gastric organoids with noted genotypes (n = 3 independent experiments). (**P**) Immunoblots of *Cdh1*$^{-/-}$ *RHOA*$^{Y42C/+}$ organoids treated for 48 h with DMSO or FAK inhibitor defactinib (2.5 μM or 5 μM) (n = 3 independent experiments). (**Q**) *In vitro* proliferation of *Cdh1*$^{-/-}$ *RHOA*$^{Y42C/+}$ organoids treated for the indicated days with DMSO or defactinib (2.5 μM). Data are mean ± S.D. ****P<0.0001, two-way ANOVA. (**R**) *In vitro* proliferation of *Trp53*$^{-/-}$*Kras*$^{G12D/+}$ organoids treated as in panel (**I**). No significance, two-way ANOVA (defactinib versus DMSO). Data are mean ± S.D.

Supplementary Figure 8 (A-H)

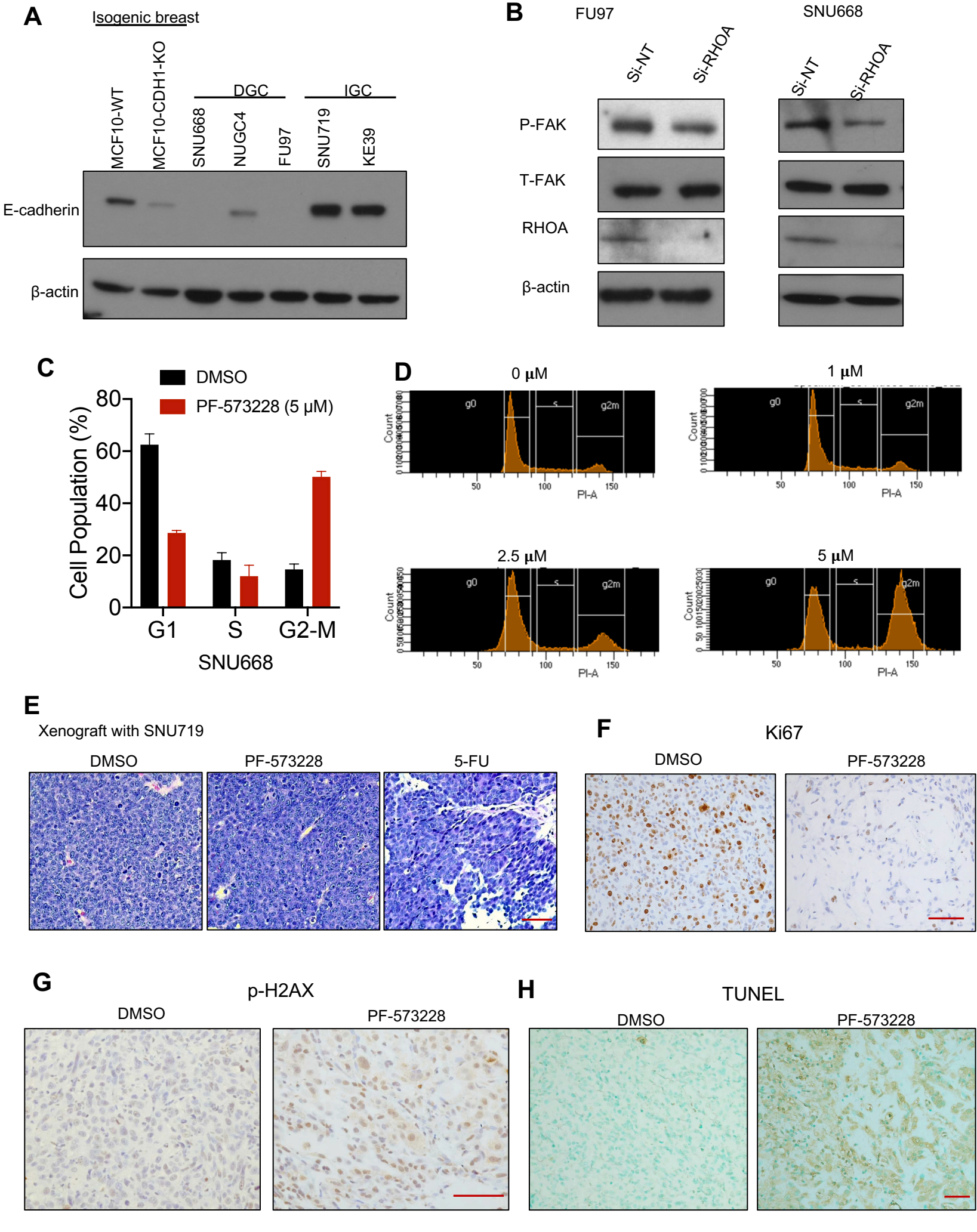

I

S08-55589:100%

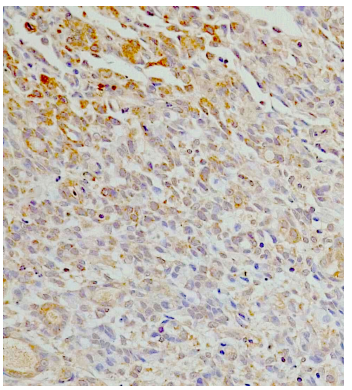

S09-53437 : 100%

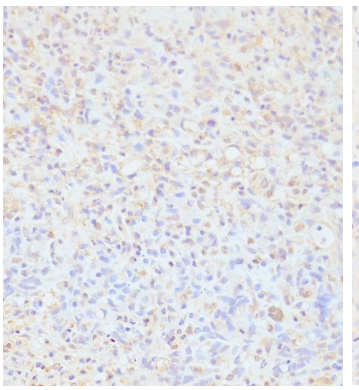

S09-59093: 70%

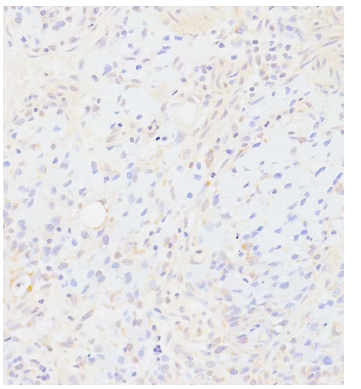

S10-3569: 100%

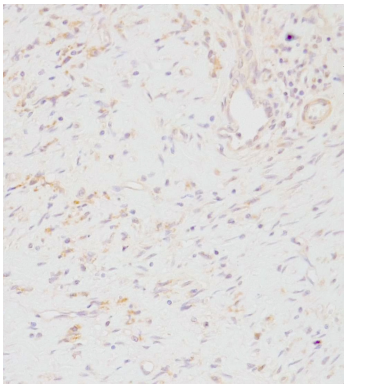

S10-9074 : 90%

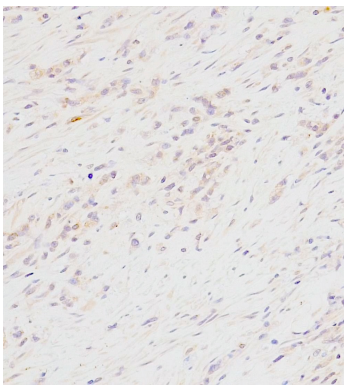

S11-54207 : 80%

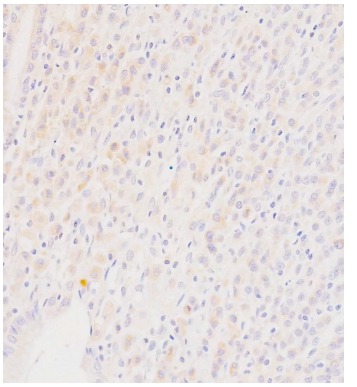

S11-56530 : 100%

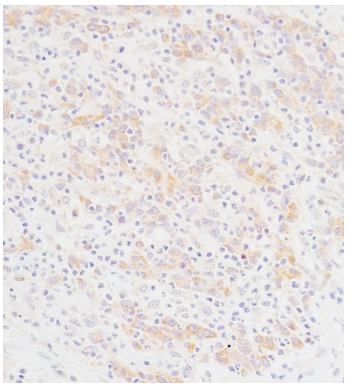

S12-00473 : 30%

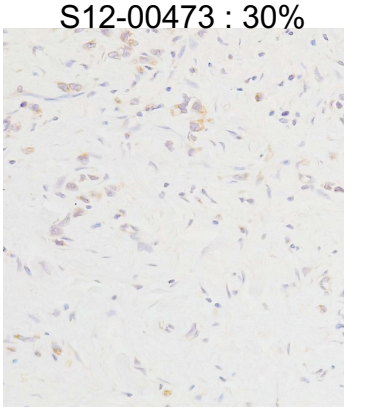

S14-07932 : 100%

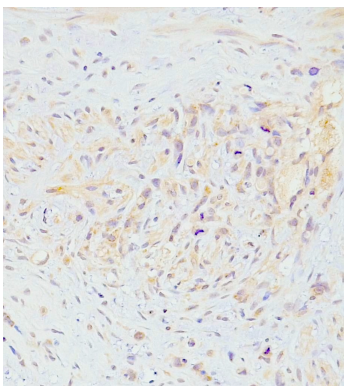

S14-45774 : 100%

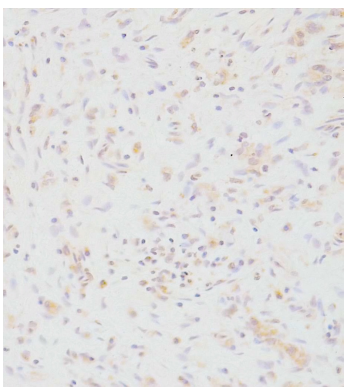

S15-02557 : 100%

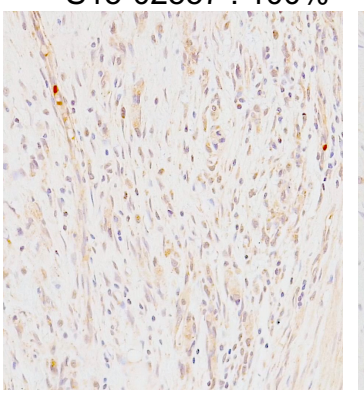

S15-04902 : 90%

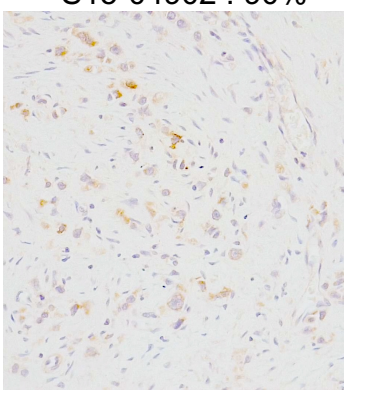

S15-08581 : 90%

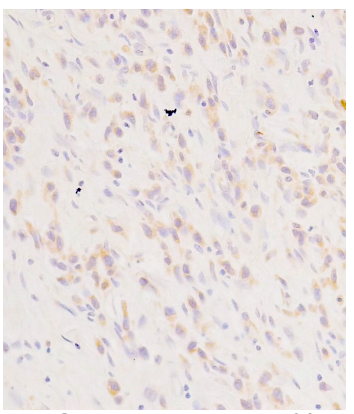

S15-62018 : 80%

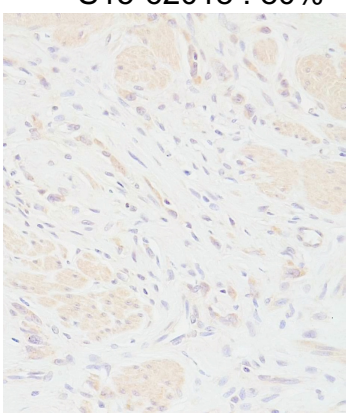

S16-42392 : 80%

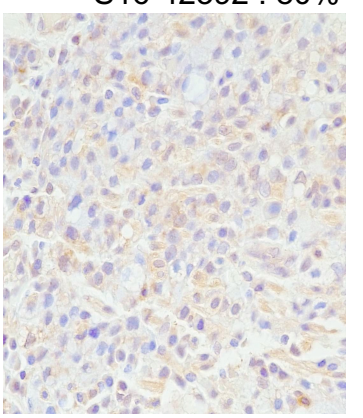

S17-37906 : 100%

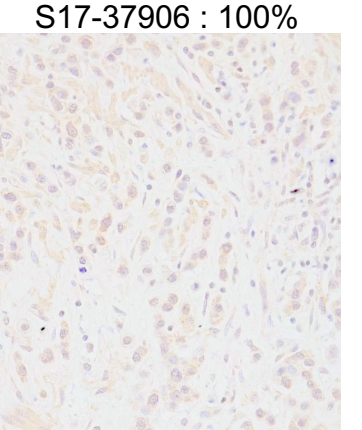

S17-38425 : 100%

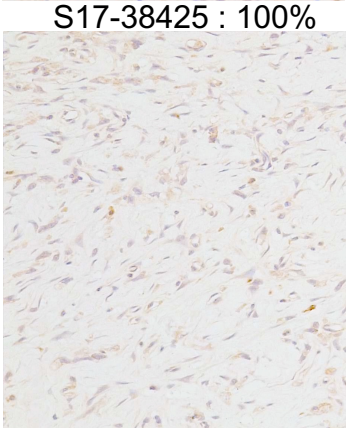

Supplementary Figure 8-I

Supplementary Figure 8-J

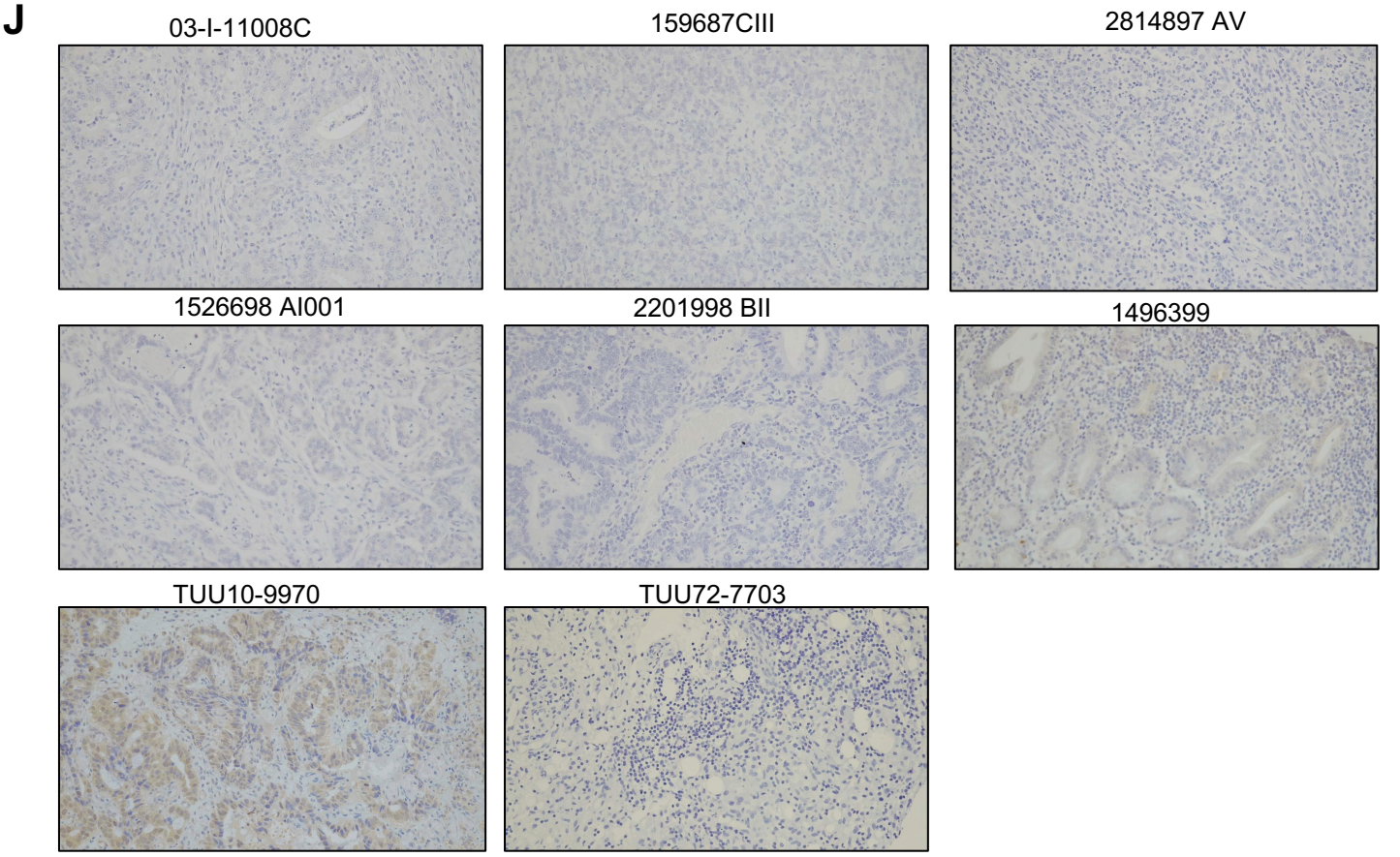

Supplementary Figure 8. FAK is activated in human diffuse gastric cancer

(**A**) Immunoblots for E-cadherin from MCF10 cells with CDH1-WT or CDH1-KO as the controls; DGC cell lines: SNU668, NUGC4 and FU97, and IGC lines SNU719 and KE39 (n = 3 independent experiments). (**B**) Representative immunoblots of FU97 and SNU668 cells with silencing of *RHOA* or Non-targeting (NT) control (n = 3 independent experiments). (**C-D**) Flow cytometry for the cell cycle analyses with SNU668 cells treated with DMSO or PF-573228 (5 μM) for 48h (**C**) or with a dose treatment (**D**). (**E**) Representative images of H&E of tumors from Fig. 7G, Scale bar = 100 μm. (**F-H**) Representative images of (**F**) Ki67 staining or (**G**) gama-H2A.X (S139) staining or (**H**) TUNEL staining of tumors from Fig.7F, Scale bar = 100 μm. (**I**) Immunohistochemistry of p-FAK staining images for tumors from all the other 17 patients of diffuse gastric cancer and the percentage of positive staining of tumor cells for each sample. (**J**) Immunohistochemistry of p-FAK staining images for tumors from 8 patients of Non-DGC.